Automated identification of clusters and UWB channel parameters dependency on Tx-Rx distance

Abdelbasset Massouri, Laurent Clavier, Jiejia Chen, Pierre Combeau, Yannis Pousset

Automated Identification of Clusters and UWB Channel Parameters Dependency on Tx-Rx Distance

Abdelbasset Massouri[1], Jiejia CHEN[2], Laurent Clavier[3], Pierre Combeau[4], Yannis Pousset[5]
Email:elmassouri@yahoo.fr[1], laurent.clavier@telecom-lille1.eu[2]
combeau@sic.sp2mi.univ-poitiers.fr[3], pousset@sic.sp2mi.univ-poitiers.fr[4]
Institut d'Electronique, de Microlectronique et de Nanotechnologie, UMR CNRS 8520, IEMN-DHS, Avenue Poincarré B.P. 60069 59652 Villeneuve d'Ascq Cedex France[1,2,3]
SP2MI, Téléport 2, Bd Marie et Pierre Curie, BP 30179, 86962 FUTUROSCOPE CHASSENEUIL Cedex, France[4,5]

***Abstract*—This paper describes the parameters of a typical impulse response generated by the ray tracer simulator developed by the SIC laboratory of POITIERS. This simulator is based on a physical model, a 3D description of the environment and ray tracing algorithm to research for the MultiPath Components (*MPC*). UWB channel consists of several MPCs arriving to the receiver in clusters. In fact, an algorithm of identification of clusters using a physical approach was implemented. Then a very particular attention was given to the evolution of the delay spread and the distribution of the received power as a function of the distance. The paper identifies also the distributions of interarrival times of clusters and MPCs within clusters.**

***Index Terms*- UWB, MPC, cluster, automated identification, delay spread, path loss**

I. Introduction

The tendency for multipath components (*MPCs*) in wide band channel impulse responses (*CIRs*) to form exponentially decaying clusters was first reported by Saleh and Valenzuela over twenty years ago [1]. Their model was later adopted by IEEE 802.15.3a and 802.15.4a task groups as the standard model for ultra wide band (*UWB*) CIRs [2], [3]. Before any S-V model parameters can be extracted, the clusters must first be identified. Past works on cluster identification have shown that performing such identification through time-consuming manual techniques can be fairly arbitrary and, if the criteria applied are slightly different, can lead to dramatically different results [4], [5].

In the proposed work, simulations are made in the frequency band from 2 to 10 GHz in a 3D description of the HALL Poitiers environment. We used angle of arrival (*AoA*) and time of arrival (*ToA*) to group the rays in clusters. The accuracy of ray tracing allows an accurate definition of the clusters. Channel simulations are done to represent node to node communication in an *ad hoc* network. We study the evolution of the channel parameters based on the IEEE 802.15.3a task group model with transmitter-receiver distance.

This paper is organized as follows. Section II describes the parameters of a typical impulse response based on the SIC[1] ray tracer simulator. Section III describes the delay spread dependency on the Tx-Rx distance, and the statistical model of small-scale fading based on the results of simulation. Finally section IV presents the algorithm of automated identification of clusters based on a real physical approach, clusters and paths interarrival times distributions.

II. Communication Ray Tracer Simulator

In wireless communication, a received signal is the result of a multipath phenomenon. This is due to electromagnetic interactions (reflection, diffraction and refraction) between an electromagnetic wave and obstacles in the environment. Each path is characterized by a specific loss, polarization, propagation delay, as well as Direction of Arrival (DoA) and Direction of Departure (DoD) in azimuth and elevation [6]. The received signal derives from the sum of all the paths. To simulate this multipath mechanism, a wave propagation simulator was developed in the SIC laboratory [7]. This allows a deterministic prediction of radio channel behavior. It associates an optimized 3D ray-tracing technique to an asymptotic frequency method, which is based on the Geometrical Optic (GO) and the Uniform Theory of Diffraction (UTD). Figure 1 shows input and output information of the wave propagation simulator. The inputs concern information about the environment (geometrical and electrical properties), antennae (position, radiation pattern, polarization and carrier frequency) and electromagnetic interactions. The output information consists of the double-directional complex CIR.
Simulation are carried out on 3D description of a large hall in the University of Poitiers. Entry is through a short corridor (around Tx1 on figure 2) and two small corridors provide an entry to an auditorium. In the center there is a 10m long and 3.5m wide room with glass walls. The total size of the environment is about $1200m^2$. Ten transmitters are randomly located in the hall. Around each receiver, four discs are defined ($0-3m$, $3-6m$, $6-9m$ and $9-12m$). In each disc, 100

[1]SIC: *Signal, Image, Communications*, Department of the XLIM, Research Institute jointly held by the University of Limoges and CNRS.

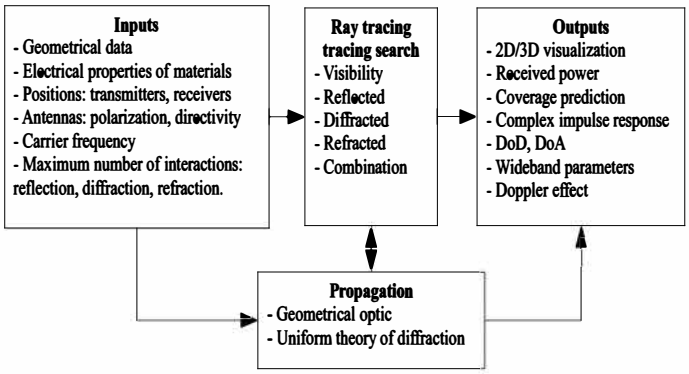

Figure 1. Inputs, Outputs and functional Description of the CRT simulator

users are randomly placed and impulse response are simulated for a total number of 4000 responses.

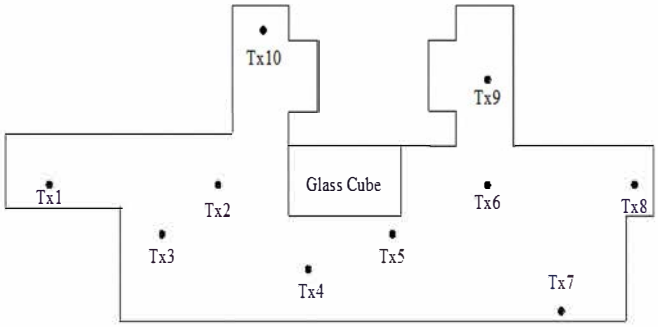

Figure 2. 2D representation of the scene and positions of transmitters

III. Channel Characterization

A. Delay Spread Dependency on Tx-Rx Distance

Delay spread is a key parameter for UWB channel statistical modeling. According to the simulation results, frequency does not have a major effect on the delay spread. In this paper we present some results which show the dependency of the delay spread on Tx-Rx distance. On figure 3 the probability density function for each disc is plotted. We notice the spreading of the density as the distance increases except for the two further discs that have similar behavior. This is confirmed by the variance values in each disc given in table I.

Area (R_{min}, R_{max})	R_{mean} (m)	Delay spread (ns)
(0,3)	2	4.7505
(3,6)	4.667	9.4586
(6,9)	7.6	10.9660
(9,12)	10.571	10.9522

Table I
COVERAGE AREAS: AND THEIR CORRESPONDENT MEAN DISTANCE AND DELAY SPREAD

This is also represented in figure 4 where the delay spread is plotted as a function of the Tx-Rx distance. On the first meters, the delay spread is low and with a small variance due

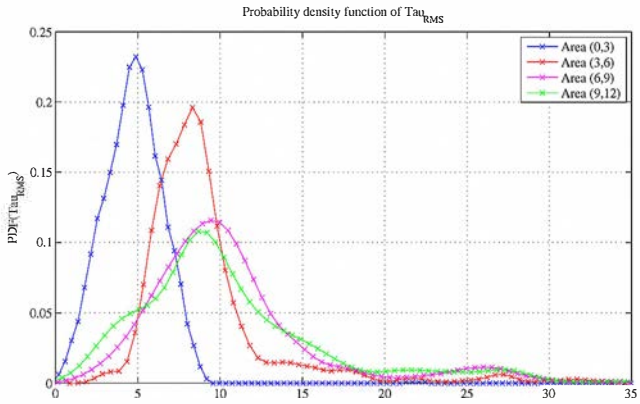

Figure 3. PDF of Delay spread dependency on Tx-Rx distance

to the dominant line of sight path. As the distance increases, the LOS path is less dominant and the influence of reflected paths get larger. Consequently, the variance is larger and high values of delay spread are frequently obtained. Between 5 and 12 meters, the variation and the mean values only slightly change.

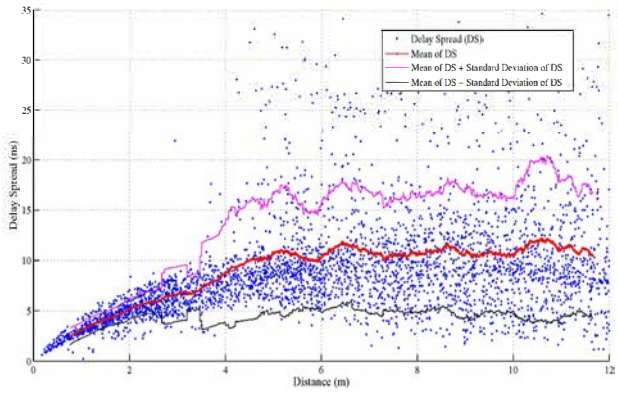

Figure 4. Delay spread dependency on Tx-Rx distance

B. Statistical Modeling of Small-Scale Fading

The channel attenuation is is affected by several factors which we summarize in the expression:

$$P_r = P_0.A_0.d^{-\gamma}.\chi_i \quad (1)$$

where P_r and P_0 are the received and transmitted powers respectively, A_0 is the average attenuation for a distance of 1 meter which takes into account the antennas gains, γ is the attenuation coefficient. We define χ_i as a random variable modeling the fluctuations around the mean attenuation $A_0.d^{-\gamma}$ due to multipath fading. χ_i can be represented by a Rice distribution which parameters vary with d. Rice fading occurs when one of the paths, typically a line of sight ray, is much

stronger than the others. The probability density function (PDF) of the Rice fading channel is given in [13]:

$$f(x|\nu,\sigma) = \frac{x}{\sigma^2} exp(-\frac{x^2+\nu^2}{2\sigma^2}) I_0(\frac{x\nu}{\sigma^2}) \quad (2)$$

where ν denotes the peak amplitude of the dominant signal, σ^2 is the variance and $I_0(z)$ is the modified Bessel function of the first kind with order zero. First, we estimate A_0 and γ (see figure 5). We find $\gamma = 2.6$ and $A_0 = -37dB$. We also notice that the variation of the attenuation increases when the distance increases.

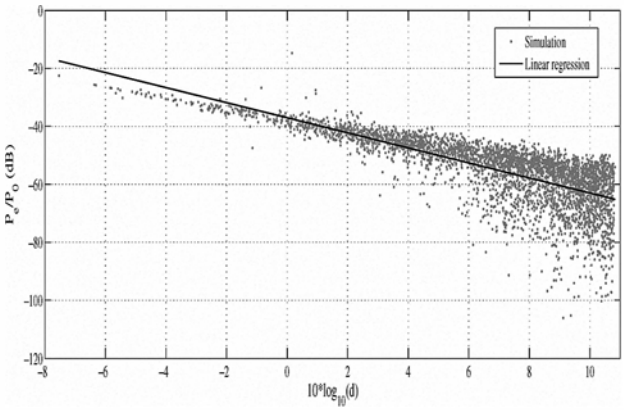

Figure 5. Received Power as a function of the distance

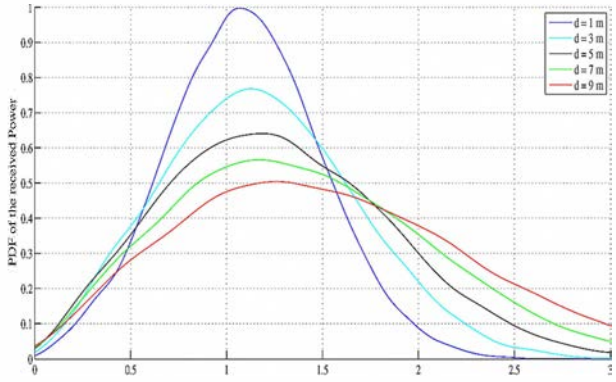

Figure 6. PDF of the received Power for various distances

In figure 6 we represent the probability density function of the received power for several Tx-Rx distances. We clearly see the increase in the spreading of the received power. To represent this evolution we plot in figure 7 the variance of the received power distribution as a function of the distance. A linear regression is well suited to represent this evolution. If v is the variance and d the distance, we can write $v = ad + b$ with $a = 0.070$ and $b = 0.335$.

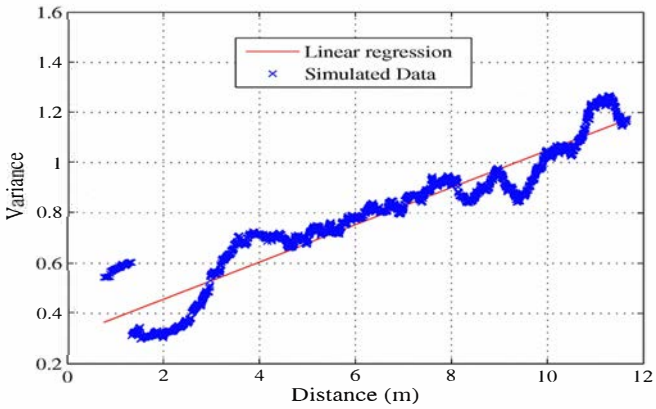

Figure 7. Linear regression of the distributed variance evolution

IV. Clusters

The considered IR in our studies is based on the S-V model which express the CIR as:

$$h(t) = \sum_{l=0}^{L} \sum_{k=0}^{K} \beta_{k,l} exp(j\phi_{k,l}) \delta(t - T_l - \tau_{k,l}) \quad (3)$$

where $\beta_{k,l}$ and $\phi_{k,l}$ are the weight the phase of the k^{th} component in the l^{th} cluster, T_l is the delay of the l^{th} cluster and $\tau_{k,l}$ is the delay of the k^{th} MPC with respect to the arrival time of the l^{th} cluster.

A. Algorithm of Automated Identification of Clusters

As suggested by Saleh and Valuenzela, our simulation results confirm the arrival of MPCs in clusters. Therefore we developed an algorithm for automated identification of clusters. The implemented algorithm is made of two steps. The key parameter of the first step is the azimuthal DoA and those of the second step are the ToA and the amplitude of MPCs of the IR.

1) First Step: listing 1 describes the first step of the developed algorithm of automated identification of clusters. The key parameter of this first step is the angle or direction of arrival of rays. Our adopted approach consists in combining rays in clusters according to their azimuthal angles of arrival. This can be explained by the existence of obstacles causing reflection of groups of rays in the same direction. In this step we first sort the rays in an ascending order according to their azimuthal AoA. A new cluster is detected when the difference between the AoAs of two consecutive rays is greater than an optimal value. The considered value of the difference between the AoAs is set to 15 degree.

Algorithm 1 :First Step

Input: $\theta_k^{DoA}\ \forall k \in [1, K]$
Output: 1- L : Number of Clusters
Output: 2- Save the L Clusters Each One in a Separate file
$l \Leftarrow 1$
$K_P^l \Leftarrow 1$
|| Sort The K Paths of The IR by Their Azimuthal DoA
for $k = 2$ to K **do**
$\Delta\theta_k^{DoA} = \theta_k^{DoA} - \theta_{k-1}^{DoA}$
if $(\Delta\theta_k^{DoA} \geq \Delta\theta_{Opt}^{DoA})$ **then**
$l \leftarrow l + 1$
|| Save Each Cluster in a Separate file
|| Save The Number of Paths of The l^{th} Cluster (K_P^l)
else
$K_P^l \leftarrow K_P^l + 1$
end if
end for
$L = l$, Save L

By applying the first step of the algorithm to a given IR, 5 clusters have been identified as shown in the left graph of figure 8.

After reviewing the PDP of this IR which consist of the five

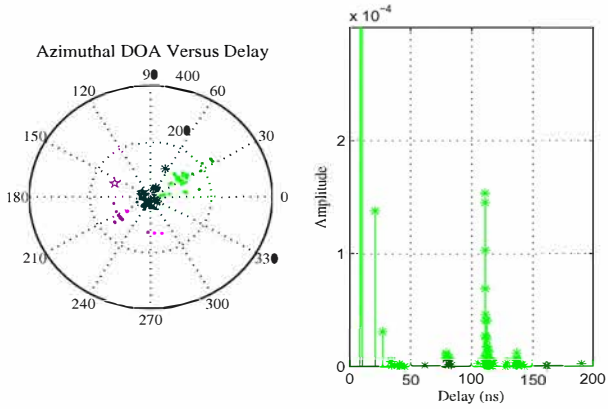

Figure 8. 5 Identified Clusters from the first step of the algorithm, each color represent a cluster. On the right side the first cluster identified in the first step still contains in fact 3 different clusters.

colored identified clusters, we can observe easily the existence of residual clusters as shown in the right graph of the same figure. As consequence we need a second step to refine the cluster identification.

2) Second Step: listing 2 describes the second step of the developed algorithm of automated identification of clusters. The key parameters of this second step are time of arrival and amplitude of rays. This step is applied to each cluster identified in the first step of the algorithm. A new cluster is detected when the delay and the amplitude ratio between two consecutive rays are greater than some optimal values. The considered values in our simulations are 5ns for the delay and 10 for the ratio. As a result of applying the second step of the algorithm we identified 9 clusters for the considered IR.

Algorithm 2 :Second Step

Input: τ_k and $\beta_k\ \forall k \in [1, K_P^l]$
Output: 1- $L^{'}$: Total Number of Clusters
Output: 2- Save the $L^{'}$ Clusters Each One in a Separate file
$l^{'} \Leftarrow L$
$K_P^{l^{'}} \Leftarrow 1$
for $l = 1$ to L **do**
|| Sort The K_P^l Paths of The l^{th} Cluster by Their ToA
for $k = 2$ to K_P^l **do**
$\Delta\tau_k = \tau_k - \tau_{k-1}$
$R_k = \frac{\beta_k}{\beta_{k-1}}$
if $(\Delta\tau_k \geq \Delta\tau_{Opt})$ and $R_k \geq R_{\beta_{Opt}}$ **then**
$l^{'} \leftarrow l^{'} + 1$
|| Save Each Cluster in a Separate file
|| Save The Number of Paths of The $(l^{'})^{th}$ Cluster
else
$(K_P^{l^{'}}) \leftarrow (K_P^{l^{'}}) + 1$
end if
end for
end for
$L^{'} = l^{'}$, Save $L^{'}$

B. Clusters Interarrival Times

In this section the arrival times of clusters is studied. The estimated distribution of the interarrival times fit an exponential distribution,

$$p(T_l|T_{l-1}) = \frac{1}{\Lambda} exp[-\frac{(T_l - T_{l-1})}{\Lambda}] \quad (4)$$

where $1/\Lambda$ is the the cluster arrival rate which is assumed to be independent of l. Λ is typically in the range of 10-50 ns [8], [9], [10], [11], [12]. An illustration of the exponential decay is given on 9.

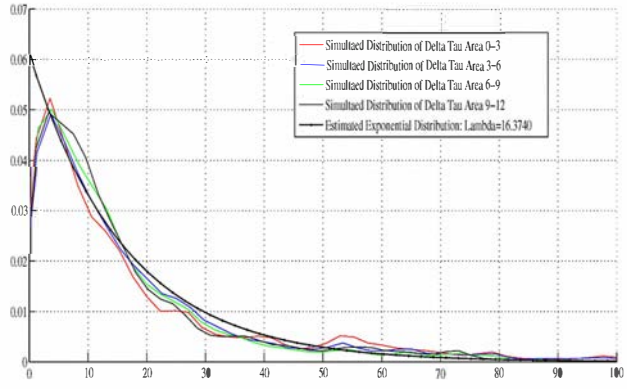

Figure 9. Distribution of Interarrival Times of Clusters

The different values of Λ for the four area are given in the table II.

Area (R_{min}, R_{max})	(0,3)	(3,6)	(6,9)	(9,12)
$\Lambda(ns)$	20.0	18.3	17.0	16.4

Table II
COVERAGE AREAS: AND THEIR CORRESPONDENT VALUE OF Λ IN NS

We can observe a slight decrease of Λ in function of coverage areas but not very significant.

C. Path Interarrival Times

For the interarrival times of MPCs within a cluster, a number different models have been proposed:
1) Regularly spaced arrival times [15], [12].
2) Poisson arrival times
3) Mixed Poisson process [4].
Based on our simulations we found that the interarrival times of MPCs within the clusters fit an exponential distribution,

$$p(\tau_k|\tau_{k-1}) = \frac{1}{\lambda} exp[-\frac{(\tau_k - \tau_{k-1})}{\lambda}] \quad (5)$$

where $1/\lambda$ is the the MPCs arrival rate which is assumed to be independent of k. An illustration of the exponential decay is given on 10.

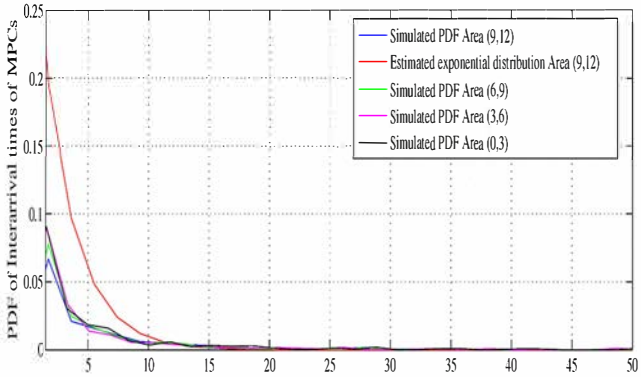

Figure 10. Distribution of Interarrival Times of MPCs within the clusters

The different values of λ for the four area are given in the table III.

Area (R_{min}, R_{max})	(0,3)	(3,6)	(6,9)	(9,12)
$\lambda(ns)$	2.5848	2.6307	2.6762	2.7273

Table III
COVERAGE AREAS: AND THEIR CORRESPONDENT VALUE OF λ IN NS

We can notice two facts about the evolution of the delays in the cluster. First the modeling with a Poisson process is not really adequate. The other solutions have to be tested, especially the third one, or new approaches have to be developed. Secondly, the law does not really depend on the distance since the change in parameter lambda is not significant. The laws of time of arrivals are not very sensitive to distance and the reasons for changes in delay spread and received power have to be found in other parameters, either the number of clusters or the amplitudes of paths.

V. CONCLUSION

UWB channel simulations based on CRT ray tracer simulator have been conducted in the frequency band of $2-10$ GHz in a 3D representation of a large hall in Poitiers under different propagation scenarios. Characterization of UWB channel shows that the received power fits a Rice distribution. The statistical analyses of the received power and of the delay spread show a clear evolution of the channel with the distance. This dependency with the distance has to be taken into account, for example in multihop strategy definitions. Clusterization phenomenon introduced by Saleh and Valuenzela was confirmed through IR simulation. Therefore an algorithm of automated identification of clusters based on physical approach was developed. Statistical analyses of clusters arrival times shows an exponential decay distribution of interarrival times of clusters. Amplitude distribution of head of clusters and paths are under study.

REFERENCES

[1] A.A.M. Saleh and R.A. Valenzuela, *"A statistical model for indoor multipath propagation,"* IEEE J.Sel. Areas Commun., vol. 5, no 2, Feb. 1987, pp. 128-137.

[2] A.F. Molisch et al., *"IEEE 802.15.4a channel model - final report,"* IEEE 802.15-04-0662-00-004a, Nov. 2004.

[3] A.F. Molisch et al., *"A comprehensive standardized model for ultrawideband propagation channels,"* IEEE Trans. Antennas Propagat., vol. 54, no. 11, pp. 3151-3166, Nov. 2006.

[4] C-C. Chong and S.K. Yong, *"A generic statistical-based UWB channel model for high-rise apartments,"* IEEE Trans. Antennas Propag., vol.53, no. 8, pp. 2389-2399, Aug. 2005.

[5] B. Kannan and F. Chin, *"Characterization of Ultra-Wideband Channels: Small-Scale Parameters for Indoor & Outdoor Office Environments,"* IEEE 802.15-04-0342-00-004a, Jul. 2004.

[6] Steinbauer, M. and Molisch, A.F. and Bonek, E. *"The double-directional radio channel,"* Antennas and Propagation Magazine, IEEE, 43(4) : 51 - 63, August 2001.

[7] Combeau, P and Aveneau, L and Vauzelle, R and Pousset, Y *"Efficient 2D Ray-Tracing Method for Narrow and Wide-band Channel Characterization in Micro-cellular Configurations,"* IET Proc., Microw. Antennas Propag., vol. 153, no. 6, pp. 502-509, Dec. 2006.

[8] B. Kannan et al. *"UWB Channel Characterization in Office Environments,"* IEEE, Tech. Rep. Document IEEE 802.15-04-0439-00-004a, 2004.

[9] B. Kannan et al. *"UWB Channel Characterization in Outdoor Environments,"* IEEE, Tech. Rep. Document IEEE 802.15-04-0440-00-004a, 2004.

[10] A. F. Molisch et al. *"A comprehensive model for ultrawideband propagation channels of UWB system proposals standard for these applications,"* Proc. IEEE Globecom, 2005, in press.

[11] D. Cassioli and A. Durantini, *"A time domain propagation model of the UWB indoor channel in the FCC-compliant band 3.6-6 GHz based on pn-sequence channel measurements,"* in Proc. VTC'04 Spring, 2004, pp. 213 - 217.

[12] D. Cassioli, M. Z. Win, and A. F. Molisch, *"The ultra-wide bandwidth indoor channel: From statistical model to simulations,"* IEEE J. Sel. Areas Commun., pp. 1247 - 1257, 2002.

[13] Eltoft, T, *"The Rician inverse Gaussian distribution: a new model for non-Rayleigh signal amplitude statistics,"* Image Processing, IEEE Transactions on, Volume 14, Issue 11, Nov. 2005, pp. 1722 - 1735

[14] C. Lemoine, P. Besnier, M. Drissi, *"Investigation of reverberation chamber measurements through high power goodness of fit tests,"* IEEE Trans. Electromagn. Compat., vol. 49, no. 4, Nov. 2007, pp.745 - 755.

[15] J. Karedal, S. Wyne, P. Almers, F. Tufvesson, and A. F. Molisch, *"Statistical analysis of the UWB channel in an industrial environment,"* in Proc. VTC Fall 2004, 2004, pp. 81-85.

[16] C. C. Chong, Y. Kim, and S. S. Lee, *"A modified S-V clustering channel model for the UWB indoor residential environment,"* in Proc. IEEE VTC Spring,05, in press.